Published in final edited form as:
Nature. 2015 June 4; 522(7554): 62–67. doi:10.1038/nature14483.

Cardiac lymphatics are heterogeneous in origin and respond to injury

Linda Klotz[1,*], **Sophie Norman**[2,*], **Joaquim Miguel Vieira**[2,*], **Megan Masters**[2], **Mala Rohling**[2], **Karina N. Dubé**[1], **Sveva Bollini**[3], **Fumio Matsuzaki**[4], **Carolyn A. Carr**[2], and **Paul R. Riley**[2,#]

[1]UCL-Institute of Child Health, Molecular Medicine Unit, 30 Guilford Street, London WC1N 1EH, United Kingdom

[2]University of Oxford, Department of Physiology, Anatomy and Genetics, South Parks Road, Oxford OX1 3PT, United Kingdom

[3]Regenerative Medicine Laboratory, University of Genoa & IRCCS AOU San Martino-IST, Largo Rosanna Benzi, 16132 Genoa, Italy

[4]Laboratory for Cell Asymmetry, RIKEN Center for Developmental Biology, 2-2-3, Minatojiima-Minamimachi, Chuou-ku, Kobe 650-0047, Japan

Abstract

The lymphatic vasculature is a blind-ended network crucial for tissue fluid homeostasis, immune surveillance and lipid absorption from the gut. Recent evidence has proposed an entirely venous-derived mammalian lymphatic system. In contrast, we reveal here that cardiac lymphatic vessels have a heterogeneous cellular origin, whereby formation of at least part of the cardiac lymphatic network is *independent* of sprouting from veins. Multiple cre-lox based lineage tracing revealed a potential contribution from the hemogenic endothelium during development and discrete lymphatic endothelial progenitor populations were confirmed by conditional knockout of *Prox1* in Tie2+ and Vav1+ compartments. In the adult heart, myocardial infarction (MI) promoted a significant lymphangiogenic response, which was augmented by treatment with VEGF-C resulting in improved cardiac function. These data prompt the re-evaluation of a century-long debate on the origin of lymphatic vessels and suggest that lymphangiogenesis may represent a therapeutic target to promote cardiac repair following injury.

In 1902, Florence Sabin proposed that the primary lymph sacs originate from the embryonic veins and then give rise to the entire lymphatic vasculature by sprouting and remodeling[1]. An alternative model of lymphatic development was proposed by Huntington and McClure

[#]Corresponding author: paul.riley@dpag.ox.ac.uk; Phone: +44 (0)1865 282366 .
[*]Joint first author contribution

Author Contributions

L.K., S.N. and J.M.V. carried out all experiments (except MI surgeries and MRI scanning), analyzed the data and contributed figures for the manuscript. K.D., S.B., M.M. and M.R. performed all MI surgeries and post-processed the hearts in preparation for immunofluorescence. F.M. provided the RIKEN Prox1-floxed mice. S.N. and C.A.C performed blinded-MRI scanning and analyzed the data. P.R.R. established the hypotheses and analyzed the data. J.M.V. and P.R.R supervised the studies and co-wrote the manuscript. All authors declare no conflicting or competing interests.

Europe PMC Funders Author Manuscripts

in 1910, who suggested that lymph sacs arise in the mesenchyme, independently of veins, via distinct progenitor cells[2]. More recent evidence has supported Sabin's model, such that trans-differentiation of venous into lymphatic endothelial cells (LECs) is now widely accepted, with the veins regarded as the sole origin of the entire lymphatic vasculature in mammals[3-7]. Studies which support a venous origin have exclusively focused to-date on the development of the systemic lymphatic vasculature. Organ-based lymphatics have received little attention and in the heart, whilst the presence of cardiac lymphatic vessels has been described[8], virtually nothing is known about their role during development or in the healthy or failing adult heart. We, therefore, sought to characterize the formation of the cardiac lymphatic vessels through developmental stages, to identify their embryonic origin and impact during organogenesis and to assess their response to pathological insult in the adult setting.

Development of the cardiac lymphatic vasculature

Whole-mount staining for early LEC markers VEGFR-3[9] and Prox1[10], revealed the emergence of lymphatic vessels at E12.5, sprouting from extra-cardiac regions proximal to the outflow tract, on the ventral side (Fig. 1a; increased magnification in 1b). At E14.5, lymphatic vessels were observed on the ventricular surface sprouting from the region of the sinus venosus, on the dorsal side (Fig. 1c; increased magnification in 1d and Extended Data Fig. 1a; increased magnification in 1b). At E16.5 the major dorsal vessels spread inferiorly from the inflow region (Fig. 1e; increased magnification in 1f), while ventrally smaller vessels arose between the atria (Extended Data Fig. 1c, d). By E18.5, the vessels continued to expand and projected towards the apex of the heart on both dorsal and ventral surfaces (Fig. 1g, h and Extended Data Fig. 1e, f). From birth (P0), the vessels developed a more extensive branched network and expanded further over the ventral side of the neonatal heart (Fig. 1i, j). By post-natal day 10 (P10), the cardiac lymphatics provided superficial coverage of the majority of the epicardial surface of the heart (Extended Data Fig. 1g, h) and appeared fully developed by P15 (Extended Data Fig. 1i, j). The lymphatic identity of the VEGFR-3 and Prox1-labeled cardiac vessels (Fig. 1a-j; Extended Data Fig. 1a-n) was further validated by co-immunostaining for the lymphatic vessel endothelial hyaluronan receptor 1 (LYVE-1), which also labels tissue-macrophages[11]. Coronary LECs within the expanding plexus on both dorsal and ventral sides of the developing heart co-expressed VEGFR-3, Prox1 and LYVE-1 (Extended Data Fig. 1o-v). Cardiac lymphatic vessels aligned with the endomucin (Emcn)-positive coronary veins during late gestation (E15.5-18.5) (Fig. 1k-m) and established extensive inter-vessel connections analogous to blood vessel anastomosis (Fig. 1n-p). At birth (P0) lateral LYVE-1+ sprouts beneath smooth muscle actin (SMA)-positive coronary veins (Fig. 1q-s) were indicative of a close anatomical relationship between the coronary veins and developing lymphatic vasculature (Fig. 1t).

A venous and non-venous contribution of LECs

Prox1+ LECs did not appear to emerge or bud-off from Emcn-expressing coronary vessels between E12.5-14.5 (Extended Data Fig. 2a-i). Instead, extra-cardiac LECs migrated into the sinus venosus on the dorsal side, and outflow tract on the ventral side of the heart by E12.5 (Extended Data Fig. 2a, b; also Fig. 1a, b) and expanded to form a network proximal

to Emcn+ veins from E13.5 and E14.5 (Extended Data Fig. 2d-i) through to E17.5 (Extended Data Fig. 2j-o). Whole embryo staining at E10.5 and E12.5 (Extended Data Figure 3a-f) revealed a Prox1/VEGFR-3-expressing LEC population emerging from the Emcn+ common cardinal vein and migrating towards the neighboring sinus venosus and outflow tract (Extended Data Fig. 3d-f), suggesting that cardinal vein ECs may be the venous source of coronary lymphatic vessels, an observation supported by previous studies[5,7].

To further investigate the lymphatic cellular origin, we first performed lineage tracing experiments using a TIE2-Cre line[12] with a R26R-EYFP reporter[13] revealed labeling of the embryonic cardinal vein at E10.5 (Extended Data Fig. 4a-d). At E12.5, Emcn+ jugular (cardinal) veins (JV) and lymph sacs (JLS), contributors to the systemic lymphatic vascular network[5], were both YFP+ and LYVE-1+ (Fig. 2a-f). In contrast, E14.5 hearts revealed lymphatic vessels proximal to the outflow tract region which were YFP-negative (Fig. 2g, h), despite complete TIE2-EYFP recombination and labeling of lymphatics elsewhere in the embryo (Extended Data Fig. 4a-c). The relative incidence of YFP+ versus YFP− lymphatic vessels in the heart was 78+/− 5.5% YFP+ versus 19+/− 3.3% YFP− cells (mean % cells +/− SEM per field of view; n=24 fields of view; 6 fields of view per heart, 4 hearts in total) and confirmed by orthogonal z-stack reconstruction (Fig. 2i), which revealed both YFP+ (Fig. 2j, k) and YFP− vessels (Fig. 2l, m) in the developing heart at E17.5.

To confirm a non-venous contribution to cardiac lymphatic vessels, we analyzed tamoxifen-inducible blood endothelial specific PDGFB-CreER^{T2} mice, crossed with either R26R-tdTomato[14] or R26R-mTmG[15] reporter lines (Extended Data Fig. 4e-o). Incomplete recombination of tdTomato within LYVE-1+ lymphatic vessels (Extended Data Fig. 4f) was evident with both Tomato+/LYVE-1+ (Extended Data Fig. 4g-i) as well as Tomato −negative/LYVE-1+ lymphatic vessels (Extended Data Fig. 4j-l), indicating a mixed contribution of endothelial- and non-endothelial-derived cardiac lymphatics. This was supported by crosses with an mTmG reporter mouse, where the level of GFP recombination within cardiac lymphatic vessels was mosaic (Extended Data Fig. 4m-o).

A hemogenic endothelial source of cardiac LECs

We next examined the possibility that an alternate source of LECs might arise from one of three potential cardiac progenitor populations[16]: the epicardium, cardiac mesoderm (early and late stage) or cardiac neural crest (CNC) by lineage tracing with Wt1-CreERT2[17], Mesp1-Cre[18], Nkx2.5-Cre[19] and Wnt1-Cre[20] lines crossed with the R26R-EYFP reporter, respectively. There was no contribution of Wt1+ (YFP+) cells to the developing coronary lymphatics, excluding the pro-epicardial organ (PEO) as a source of LECs (Extended Data Fig. 5a-c) and neither Mesp1+ or Nkx2.5-labelled lateral plate mesoderm (LPM)-derived progenitors (Extended Data Fig. 5d-i) nor Wnt1+ CNC cells (Extended Data Fig. 5j-l) contributed to the developing coronary lymphatics. Subsequently, we sought to determine whether there might be a distinct TIE2-negative endothelial source of LEC progenitors. The hemogenic endothelium represents the site of primitive hematopoiesis in the visceral yolk sac and developing blood islands of the early embryo and whilst TIE2-Cre does label a significant proportion of cells within the yolk sac, there are aggregations and primitive

hematopoietic derivatives which are TIE2 negative[21]. To potentially capture this TIE2-negative population, we employed three Cre-driver lines under the control of *Vav1*[22-24], *Pdgfrβ*[25] and *Csf1r*[26], in combination with either the R26R-tdTomato or R26R-mTmG reporters. Initially we excluded reporter labelling of the endothelium of the common cardinal vein by these three drivers at E10.0 (Extended Data Fig. 6a-d and data not shown) and jugular vein at E12.5 (Extended Data Fig. 6e-h), however, we cannot exclude the possibility of tracing a subset of venous-derived cells fated to form LECs prior to any evidence of Prox1 expression. Extensive labeling of Vav1-tdTomato+ cells was evident in regions of the developing heart at E17.5 (Fig. 3a), including Tomato+/LYVE-1+ tissue macrophages (Fig. 3a), which were negative for Prox1 and located proximally to the developing vessels (Fig. 3b, c). In contrast to the situation in the heart, Vav1-tdTomato positive cells were not observed in the dermal lymphatics from dorsal skin preparations analyzed at E17.5 (n=4 embryos; Extended Data Fig. 5m-r). Subsequently, we confirmed the presence of Tomato+ cells within lymphatic vessels which were Prox1+ and LYVE-1+ (Fig. 3a, b, d; 14 +/− 5.3% Tomato+/Prox1+ (mean % cells +/− SEM per field of view; n=20 fields of view; 5 fields of view per heart, 4 hearts in total) as confirmed by z-stack reconstruction (Fig. 3a). In PDGFRβ-Cre;R26R-mTmG reporter mice, GFP+ cells were observed in the coronary lymphatics at E17.5 (Fig. 3e) which were positive for Prox1 (Fig. 3f, g) and VEGFR-3 (Fig. 3h; 28 +/− 4.7% GFP+/Prox1+; mean % cells +/− SEM per field of view; n=18 fields of view; 6 fields of view per heart, 3 hearts in total) (Fig. 3e, with z-stack) and in hearts derived from CSF1R-CreER;R26R-tdTomato embryos, a contribution of Tomato+ cells which co-labelled with Prox1 (Fig. 3i with z-stack) and LYVE-1 (Fig. 3j-l with z-stacks), further suggested a yolk-sac progenitor contribution (Fig. 3i-l). The relative incidence of Tomato+/Prox1+ cells was low (less than 5%) likely reflecting inefficient labelling by the inducible CSF1R-CreER.

In order to further investigate a yolk sac contribution to LECs, we derived ex-vivo cultures of explanted Vav1-Cre;R26R-tdTomato concepti at E8.0[27]. Intact yolk sac explants were treated with 100ng/mL of recombinant VEGF-C-Cys(156)Ser[28], a potent selective lymphangiogenic cue that only signals via VEGFR-3 (the Cys156Ser mutation prevents binding to VEGFR-2). A Tomato+ outgrowth from the yolk sac was observed under VEGF-C induction (Extended Data Fig. 6i, j) with specification of Prox1+ LECs in culture (Extended Data Fig. 6k-z). Since this stage of development was too early to detect a venous origin or alternate embryonic source, we conclude that these LECs were yolk sac-derived.

Prox1 loss of function supports dual LEC origin

To provide further evidence for both a venous-endothelium and independent source of cardiac LECs, we genetically deleted *Prox1* independently in both the TIE2+ blood endothelial and Vav1+ compartments. We first utilized *Prox1* conditional mice[29] crossed with the TIE2-Cre mice (Extended Data Fig. 7a). FACS of targeted GFP+ cells from isolated TIE2-Cre;Prox1$^{fl/fl}$ hearts (Extended Data Fig. 7b) revealed appropriate knock-down of *Prox1* (Extended Data Fig. 7c; 0.59-fold; n=5 mutant hearts analyzed; $p \leq 0.05$), accompanied by knock-down of *Vegfr3* (Extended Data Fig. 7d; 0.39-fold; n=5 mutant hearts analyzed; $p \leq 0.01$) and *Lyve-1* (Extended Data Fig. 7e; 0.22-fold; n=5 mutant hearts analyzed; $p \leq 0.001$). TIE2-Cre;Prox1$^{fl/fl}$ mutant embryos had gross vascular anomalies,

including ectopic surface blood vessels, a disrupted vascular network and apparent hemorrhaging (Extended Data Fig. 7f-i). An initial failure in specification of cardiac LECs was confirmed at E14.5, coincident with the first emergence of the lymphatics on the dorsal surface of the heart (Fig. 1c). GFP+-targeted and LYVE-1+ LECs were observed at the base proximal to the atrioventricular region of the heart in TIE2-Cre;Prox1$^{fl/+}$ controls but were absent in the mutant hearts (Extended Data Fig. 8a-f). There was no apparent effect on the coronary vasculature, as determined by comparable whole-mount CD31 staining (Extended Data Fig. 8g, h). At E17.5 TIE2-Cre;Prox1$^{fl/fl}$ hearts were recovered largely devoid of VEGFR-3+ LECs (Extended Data Fig. 9a-d) and were relatively dysmorphic along the apical-basal (long) axis (Extended Data Fig. 9c, d), with smaller chambers and thickening of the ventricular compact layer (Extended Data Fig. 8i, j). Despite these anomalies, endocardial cushions formation appeared unaffected (Extended Data Fig. 8i, j). Relative to TIE2-Cre;Prox1$^{fl/+}$ heterozygotes (Extended Data Fig. 9e-h), GFP+/LYVE-1+ lymphatic vessels were either partially or completely absent from the dorsal surface and completely absent from the ventral surface of mutant hearts (Extended Data Fig. 9i-p). The partial and complete loss of LECs correlated with the loss of Prox1 protein expression (Extended Data Fig. 9k, o). TIE2-Cre;Prox1$^{fl/fl}$ mutant hearts were also recovered at E17.5 with significant coverage of targeted GFP+/LYVE-1+ lymphatics which correlated with incomplete knockdown of *Prox1* (Extended Data Fig. 7c). The resultant phenotype was mild hypoplasia of the lymphatic vessels and a partially truncated vascular network (Extended Data Fig. 10a-f). Vessels were significantly shorter and thinner with increased truncations relative to controls (Extended Data Fig. 10m-o). Cleaved caspase 3 immunostaining revealed an increase in apoptotic cells within the termini of mutant vessels (Extended Data Fig. 8k, l) supporting the requirement for Prox1 in LEC identity and maintenance. Nevertheless, hypomorphic TIE2-Cre;Prox1$^{fl/fl}$ mutants were recoverable at post-natal stages, whereby hypoplasia of the cardiac lymphatics appeared to be rescued beyond birth (Extended Data Fig. 8m-p).

We next targeted *Prox1* within the Vav1+ lineage. Specification of lymphatic vessels in severely affected TIE2-Cre;Prox1$^{fl/fl}$ hearts at the base of the heart on the dorsal surface (Extended Data Fig. 9c, l), corresponded to the potential contribution of Vav1+ to the cardiac lymphatics (Fig. 3). In Vav1-Cre;Prox1$^{fl/fl}$ mutant hearts at E14.5, emerging VEGFR-3+ cardiac lymphatics were evident on both ventral and dorsal surfaces (Extended Data Fig. 8q-x). At E17.5 control Vav1-Cre;Prox1$^{fl/+}$ mice revealed appropriate targeting of GFP+ LECs and an extensive lymphatic network on the ventral surface as indicated by LYVE-1, with retained Prox1 expression (Extended Data Fig. 9q-s). Vav1-Cre;Prox1$^{fl/fl}$ mutants revealed no obvious systemic vessel defects (Extended Data Fig. 7j-m). Co-expression of GFP+/LYVE-1+ was observed in LECs (Extended Data Fig. 9t-x), however, specific loss of LYVE-1+ LECs was detected at sub-cellular resolution that directly correlated with loss of Prox1 and GFP-targeting (Extended Data Fig. 9y, z), supporting a Prox1-dependent Vav1+ source of cardiac lymphatics.

Neo-lymphangiogenesis post-cardiac injury

Lymphangiogenesis in other settings (most notably during skin infection) has been implicated in antigen clearance and inflammatory resolution[30,31]. Thus, we determined

whether the cardiac lymphatics might attempt compensatory angiogenesis during the pro-inflammatory phase following MI[32]. We first analyzed VEGFR-3 protein levels as a surrogate for an early lymphatic response, and observed a significant increase in VEGFR-3 at all stages from 24 hours up to day 21 post-MI (Fig. 4a). Alterations in VEGFR-3 protein were recapitulated at the gene expression level (Fig. 4b) and a general activation of the developmental lymphatic gene program was confirmed by concomitant increased expression of *Lyve1* and *Prox1* (Fig. 4c, d). At day 7 following injury there was a significant increase in the branching of surface VEGFR3+ lymphatic vessels (Fig. 4e, f), and alignment of Prox1+ lymphatic sprouting with Emcn+ veins (Fig. 4g). Longitudinal analyses, from days 7 to 35 post-MI, revealed marked spatiotemporal changes in the lymphatic response. In the intact heart there were few superficial lymphatic vessels detectable (Fig. 4h, i), as evident from staining for LYVE-1 and Podoplanin (PDPN [33]) as compared to day 7 after injury when there was a significant increase in the number of LYVE-1+/PDPN+ lymphatic vessels in cross-section, (Fig. 4j, k). These vessels increased in diameter by day 14, concurrent with nascent lymphatic network expansion (Fig. 4l, m), and persisted through day 21 (Fig. 4n, o) to day 35, where enlarged lymphatic shunts were evident, localized superficially in the myocardium at the border zone of the infarct/scar region (Fig. 4p, q). Thus, the adult cardiac lymphatics undergo significant angiogenesis following initiation of a developmental programme in response to ischemic injury.

VEGF-C improves cardiac function post-MI

To investigate the influence of neo-lymphangiogenesis on cardiac function after MI, we treated wild-type or *Vegfr3*$^{LacZ/+}$ reporter mice[34] with recombinant VEGF-C-Cys(156)Ser[28] at days 0, 2, 3, 4 and 6 post-MI. At day 7 post-MI, a stronger lymphangiogenic response (X-gal+/VEGFR3+/Prox1+) was observed surrounding the injury area in VEGF-C-treated samples, compared to vehicle-treated controls (Fig. 4r-w). Moreover, VEGF-C-treated mice exhibited a significant improvement in cardiac function as determined by longitudinal magnetic resonance imaging (MRI; Fig. 4x-z; Supplementary Table 1). Specifically, smaller ventricular end-systolic volumes (Fig. 4x, y; Supplementary Table 1) and significant improvement in the ejection fraction were recorded in the VEGF-C-treated group (Fig. 4z; Extended Data 1: 43±5 for vehicle versus 57±4 for VEGF-C-treated by 14 days post-MI; 45±5 for vehicle versus 60±5 for VEGF-C-treated by 21 days post-MI; mean ± SEM; n=8 animals per group; $p \leq 0.05$). The improvement in cardiac function was maintained for at least 28 days post-MI (Supplementary Table 1). Collectively, these data suggest that promotion of growth factor-induced lymphangiogenesis is possible in the adult diseased heart and improves prognosis, analogous to what has been reported in other disease models[35].

Discussion

Our study challenges the unequivocal view of lymphatic vessel development derived from Sabin's venous origin model[1]. We reveal that the lymphatic vasculature of the embryonic mouse heart comprises a heterogeneous make-up of cell populations, with contributions derived from both extra-cardiac venous endothelium and a novel source of lymphatic progenitors which may arise from the yolk sac hemogenic endothelium. Targeting of *Prox1*

in both venous endothelial and non-venous-derived compartments resulted in loss of the cardiac LECs, supporting a dual origin in the developing heart and consistent with previous studies demonstrating that *Prox1* is both necessary and sufficient to drive LEC fate specification[36-39]. Prox1 acts at the decision point between blood and lymphatic endothelial cell specification[40], such that *Prox1*-deficient LECs contributing to the systemic blood vasculature resulted in ectopic vessels and hemorrhaging throughout the embryo. However, in Tie2-Prox1 mutant hearts, hypoplasia of the lymphatic vessels did not appear to impact upon the gross development of the coronary blood vessels, highlighting a further unique ontology of the cardiac lymphatics relative to systemic lymphatic vasculature. Previously, *Prox1* dosage effects underpinned formation of the systemic lymphovenous valves[41]; here partial *Prox1* knockdown resulted in formation of the cardiac lymphatics but with truncation of the developing plexus and aberrant remodelling suggesting a novel role for Prox1 in maintaining the cardiac lymphatic network.

Insight into the embryological origin and development of the cardiac lymphatics has important implications for understanding cardiovascular tissue fluid homeostasis, injury-induced inflammation and disease. Following MI the cardiac lymphatics underwent a profound angiogenic response, accompanied by an up-regulation in the lymphatic development gene program. Significantly, this was enhanced by ectopic VEGF-C stimulation following injury, leading to improvement in cardiac function. Myocardial injury is associated with a robust immune reaction, characterized by sequential mobilization of monocytes involved in inflammatory functions and wound healing, respectively[32]. Lymphangiogenesis in inflammatory settings facilitates the resolution of tissue edema and promotes macrophage mobilization[30,31] and induction by VEGF-C alleviates inflammation in mouse models[42,43]. Therefore, mechanisms coupling lymphatic development to immune regulation represent a therapeutic target. Induction of lymphatic vessels could provide a pathway for inflammatory cell efflux to tip the balance in favor of wound healing within the injured adult heart.

Methods

Mouse strains

The following mouse strains were used as previously described: Csf1r-CreER[26], Mesp1-Cre[44], Nkx2.5-Cre[19], Pdgfb-CreERT2[45], PDGFrβ-Cre[46], Prox1$^{fl/+}$[29], R26R-EYFP[13], R26R-mTmG[15], R26R-tdTomato[14], Tie2-Cre[12], Vav1-Cre[47], Wt1-CreERT2[17], Wnt1-Cre[20], Vegfr3$^{LacZ/+}$[34]. Breeding was carried out using only Cre^{+} males for all Cre-strains except the Vav1-Cre where Cre^{+} females were used. Pregnant females crossed to inducible Cre male studs were injected intraperitoneally at E7.5 (Csf1r-CreER) or E9.5 (Wt1-CreERT2; Pdgfb-CreERT2) with 2mg of 4-hydroxytamoxifen (4-OHT) dissolved in peanut oil. Embryonic staging (E) was determined by the day of the vaginal plug (E0.5). C57BL/6 mice were used for the longitudinal cardiac cine-MRI study. Investigators were blinded to genotype and treatment groups. All animal experiments were carried out according to UK Home Office project license PPL 30/2987 Compliant with the UK Animals (Scientific Procedures) Act 1986.

Quantitative real-time PCR

Total RNA was isolated from hearts using the Qiagen RNeasy Mini Kit (Qiagen). cDNA was synthesized using the Reverse Transcription System (Promega), following the manufacturer's instructions and used for quantitiative real-time PCR using SYBR Green on an ABI 7900 for the following genes: *Vegfr3, Prox1, Lyve1*. Fold change was determined by applying the $2^{-\Delta\Delta CT}$ method. The following primer sequences were used: *Vegfr3*, 5′-CCATCGAGAGTCTGGACAGC-3′ forward, 5′-CCGGGATGGTGGTCACATAG-3′ reverse; *Prox1* 5′-GAAGGGCTATCACCCAATCA-3′ forward, 5′-TGAACCACTTGATGAGCTGC-3′ reverse; *Lyve1* 5′-GGCTTTGAGACTTGCAGCTATG-3′ forward, 5′-GCAGGAGTTAACCCAGGTGT-3′ reverse.

Western blotting

Heart samples were lysed in RIPA buffer (50mM Tris-HCl at pH7.6, 150 nM NaCl, 1%NP-40, 0.5% DOC, 0.1% SDS) supplemented with protease inhibitors (Protease Inhibitor Cocktail Tablet (Roche), 1mM PMSF (Sigma) and 1 μg/mL aprotinin (Sigma)). The lysate was centrifuged at 13,000×g for 15 min at 4°C and the supernatant recovered. For SDS-PAGE samples were incubated with an equal volume of 2 × Laemmli Buffer/5% β-ME at 95°C for 5 min before being resolved on a 10/15% acrylamide gel (Sigma) and analyzed by western blot using a primary antibody for VEGFR-3 (goat anti-mouse, 1 in 1000 dilution) or GAPDH (goat anti-mouse, 1 in 1000 dilution, Millipore). All secondary antibodies were conjugated to HRP and imaged using enhanced chemiluminescence (all GE Healthcare).

Immunohistochemistry and histology, confocal imaging and quantitation

Hearts and embryos for histology were collected, fixed in 2% PFA overnight and either stored in PBS, or embedded in either paraffin wax or OPT (both Raymond Lamb). 10 μm paraffin sections were stained with hematoxylin (Sigma) and eosin (Raymond Lamb). Immunofluorescent staining on 8 μm frozen sections was performed using primary antibodies to ENDOMUCIN (catalogue number SC-53941, Santa Cruz Biotechnology, 1:50 dilution), CD31 (553370, BD Pharminigen, 1:50), PROX1 (11-002, AngioBio, 1:200), PROX1 (AF2727, R&D Systems, 1:200), LYVE-1 (NBP1-43411, Novus Biologicals, 1:500), LYVE-1 (11-034, AngioBio, 1:200), VEGFR-3 (AF743, R&D Systems, 1:50), GFP (ab13970, Abcam, 1:2000), PODOPLANIN (10R-P133a, Fitzgerald, 1:500), αSMA (C6198, Sigma, 1:200), CLEAVED CASPASE-3 (9661/9664, Cell Signalling Technology, 1:100). AlexaFluor secondary antibodies (Invitrogen, 1:200) were used in all cases. The same protocol was applied to whole mount hearts and embryos with primary and secondary antibody incubations extended to overnight. Whole mount 3,3′-diaminobenzidine (DAB) staining was performed on embryonic and postnatal hearts using the Vectastain Elite ABC Kit Goat IgG and the DAB Peroxidase Substrate Kit (both Vector Laboratories) following the manufacturer's instructions. Hearts from *Vegfr3*$^{LacZ/+}$ mice were collected post-MI and stained for β-galactosidase (β-gal) activity. Briefly, hearts were fixed on ice for 30 minutes in 2% formaldehyde solution containing 0.2% glutaraldehyde (both Sigma), washed twice with phosphate-buffered solution (PBS) on ice, and stained overnight at room temperature in X-gal staining solution containing 4mM K4Fe(CN)6, 4mM K3Fe(CN)6, 2mM MgCl2 and

1mg/mL X-gal (dissolved in N-dimethylformamide; Sigma). Immunofluorescence staining was imaged using an Olympus FV1000 confocal microscope. Maximum intensity Z-projections of whole hearts were acquired using both the tiling and Z-stack functions. DAB and β-gal staining was imaged using a Zeiss stereo microscope. All images were processed using Image J software. Analysis of vessels and branching calculations were performed using AngioTool[48]. Cell lineage contribution was quantified by counting $Prox1^{+}$reporter^{+} nuclei versus Prox1+ single positive nuclei within vessels across several fields of view per heart analyzed.

Flow cytometry

Isolation of $EGFP^{+}$ cells from Tie2-Cre;Prox1-$EGFP^{fl/+}$ and Tie2-Cre;Prox1-$EGFP^{fl/fl}$ hearts and RNA extraction was performed according to standard protocols.

Yolk sac explants

E8.0 explants including the intact yolk sac were cultured for five days in Dulbecco's Modified Eagle Medium with 20% fetal calf serum and 10^{-5} mol/L 2-mercaptoethanol (Life Technologies) supplemented with 100 ng/mL of recombinant human VEGF-C (Cys156Ser) (R&D systems).

Murine cardiac injury model

$Vegfr3^{LacZ/+34}$ or C57BL/6 female mice were subject to surgery between 8 and 10 weeks, with a weight of 17-23 grams. Mice were anesthetized with 2.5% isofluorane and placed under assisted external ventilation through the insertion of an endotracheal tube. Cardiac injury was induced by permanent ligation of the left descending artery (LAD). LAD ligation mice were directly compared with sham-operated animals which underwent tracheotomy, opening of the chest and insertion of the needle trough the LV but no suture ligation. Buprenorphine (buprenorphine hydrochloride; Vetergesic) was delivered as a 0.015 mg/mL solution via intraperitoneal injection at 20 min before the procedure to provide analgesia. On recovery mice were randomly allocated to receive an intraperitoneal injection of 0.1 μg/g recombinant human VEGF-C (Cys156Ser) (R&D systems) or PBS. Further injections were administered at 2, 3, 4 and 6 days post-surgery. Experimenters were blind to treatment groups for subsequent cardiac cine-MRI and analysis. Hearts were collected at 1, 2, 4, 7, 14, 21, 28 and 35 days post-myocardial infarction (MI) and either sectioned or left intact and prepared for histology, immunofluorescence, RNA and protein extraction. Mice were housed and maintained in a controlled environment. All surgical and pharmacological procedures were performed in accordance with the Animals (Scientific Procedures) Act 1986, (Home Office, UK).

Cardiac cine-MRI

Cardiac cine-MRI was performed post-LAD ligation as described[49]. Briefly, mice were anesthetized with 2% isoflurane in O_2 and positioned supine in a purpose-built cradle. ECG electrodes were inserted into the forepaws and a respiration loop was taped across the chest. The cradle was lowered into a vertical-bore, 11.7 T MR system (Magnex Scientific, Oxon, United Kingdom) with a 40 mm birdcage coil (Rapid Biomedical, Würzburg, Germany) and

a Bruker console running Paravision 2.1.1 (Bruker Medical, Ettlingen, Germany). A stack of contiguous 1 mm thick true short-axis ECG -gated cine-FLASH images were acquired to cover the entire left ventricle (TE/TR 1.43/4.6 ms; 17.5° pulse; field of view 25.6 × 25.6 mm; matrix size 128 × 128 zero filled to 256 × 256 giving a voxel size of 100 × 100 × 1000 μm; 20 to 30 frames per cardiac cycle). Long-axis two-chamber and four-chamber images were also acquired.

MRI data analysis

Blinded image analysis was performed using ImageJ (NIH Image, Bethesda, MD). Left ventricular mass, volumes and ejection fraction were calculated as described[50]. The relative infarct size was calculated from the average of the endocardial and epicardial circumferential lengths of the thinned, akinetic region of all slices, measured at diastole, and expressed as a percentage of the total myocardial surface[50].

Statistical analysis

Statistical difference between groups was evaluated using Student's *t*-test (two-tailed) or one-way ANOVA. A *P*-value of <0.05 was considered statistically significant. All values and graphs present the mean value ± standard error of the mean (s.e.m.).

Extended Data

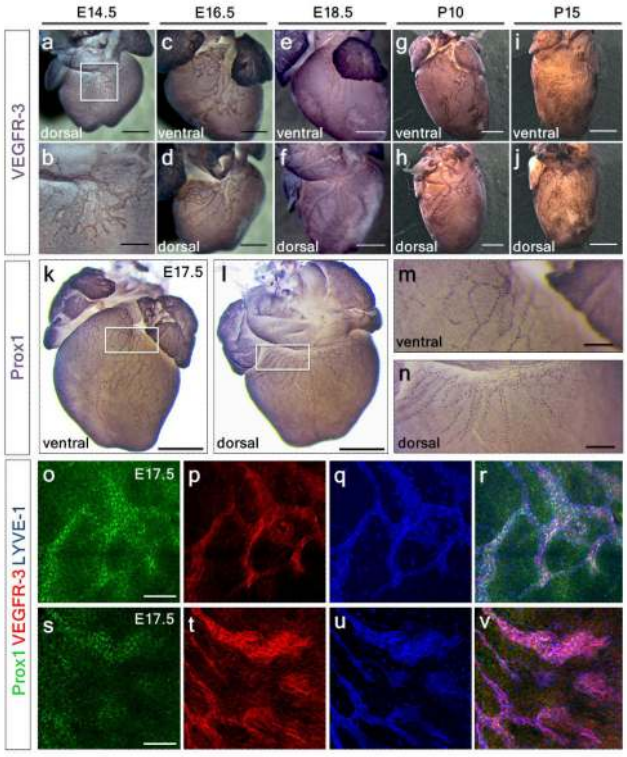

Extended Data Figure 1. Molecular characterization of the murine cardiac lymphatic vasculature

Whole-mount DAB staining of hearts (n= 3 per time point) with the lymphatic marker VEGFR-3 revealed cardiac lymphatics vessels first sprout from the region of the sinus venosus, on the dorsal side of the heart at E14.5 (**a**, white box, enlarged in **b**). At E16.5, ventrally the first small vessels arose between the atria (**c**), while the main dorsal vessels spread inferiorly from the sinus venosus at the inflow region of the heart (**d**). At E18.5 the network appears similar with little expansion (**e**, **f**). From birth, post-natal day (P) 0, lymphatic vessels branch and expand onto the ventral epicardial surface of the heart such that by P10 the network has expanded significantly coincident with cardiac growth (**g**, **h**). Consistent with the systemic lymphatic vasculature, cardiac lymphatic vessels are fully developed by P15 (**i, j**), with no difference in vessel density at later stages (data not shown). Whole-mount DAB staining of E17.5 hearts with the lymphatic marker Prox1 (n=4) further confirmed extensive spread of the sprouting lymphatics inferiorly from the outflow tract region (**k**) and sinus venosus, at the inflow region of the heart (**l**). White inset box in (**k**, **l**) is shown in (**m**, **n**; respectively) highlighting the punctate nuclear expression of Prox1 in coronary lymphatics. Whole-mount confocal imaging of E17.5 hearts (n=4) stained with VEGFR-3, Prox1 and LYVE-1 confirmed co-labelling of coronary lymphatic vessels (**o**-**v**). Note that whilst at this developmental stage VEGFR-3 is restricted to LECs (**p**, **t**), Prox1 is also expressed in the underlying myocardium (**o**, **s**) and LYVE-1 labels tissue-resident macrophages (**q**, **u**). Scale bars: **a** 750μm; **b** 300μm; **c**, **d** 750μm; **e**, **f** 1mm; **g**, **h** 2mm; **i**, **j** 2.5mm; **k**, **l** 400μm; **m**, **n** 200μm; **o**, **s** 100μm.

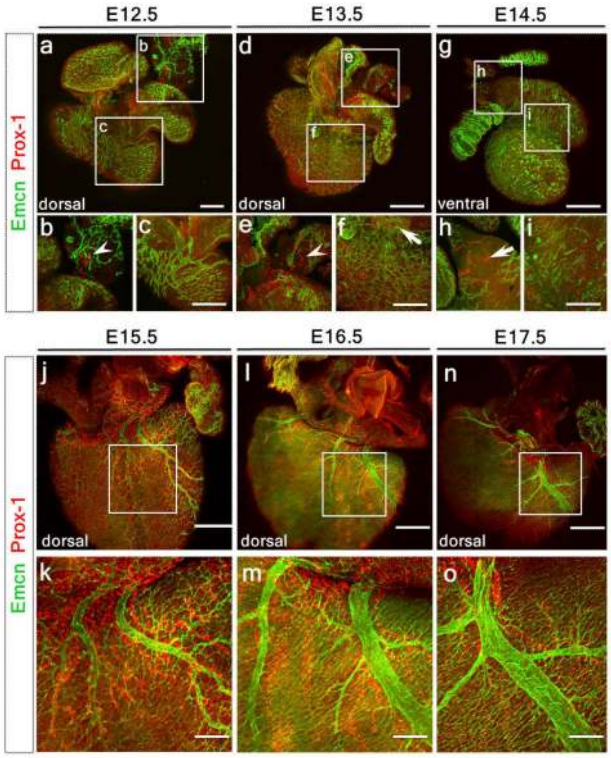

Extended Data Figure 2. Cardiac lymphatic vessels do not emerge from the developing coronary vasculature

Whole-mount confocal imaging of hearts stained with Emcn (vessels) and Prox1 (lymphatics) (**a-o**), revealed sprouting of Prox1+ lymphatics from extra-cardiac tissue neighboring the sinus venosus on the dorsal side of the developing heart at E12.5-13.5 (**a, d**), but no Prox1+ LECs were observed budding from Emcn+ coronary vessels (**c**; enlarged white inset box shown in **b** and **e**, respectively; white arrowheads in **b** and **e** highlight Prox1+ LECs). Prox1+ lymphatics had reached the sinus venosus by E13.5 (white arrow in **f**) and the outflow tract, on the ventral side of the heart by E14.5 (white arrow in **h**); no Prox1+ LECs were observed emerging from Emcn+ vessels on the ventral side at E14.5 (**g**; white box in **i**). Background-like labeling on the ventricular surface in **c, f, i** reflects Prox1 expression in the developing myocardium. Between E15.5-17.5, Prox1+ lymphatics aligned with Emcn+ coronary veins but no contribution of Prox1+ LECs was observed (**j**, **l** and **n**, white box enlarged in **k**, **m** and **o,** respectively; n=5 hearts analyzed per time point). Scale bars: **a**, 550μm; **c**, **f**, **i**, 250μm; **d**, **g**, 750μm; **j**, **l**, **n**, 400μm; **k**, **m**, **o**; 200μm.

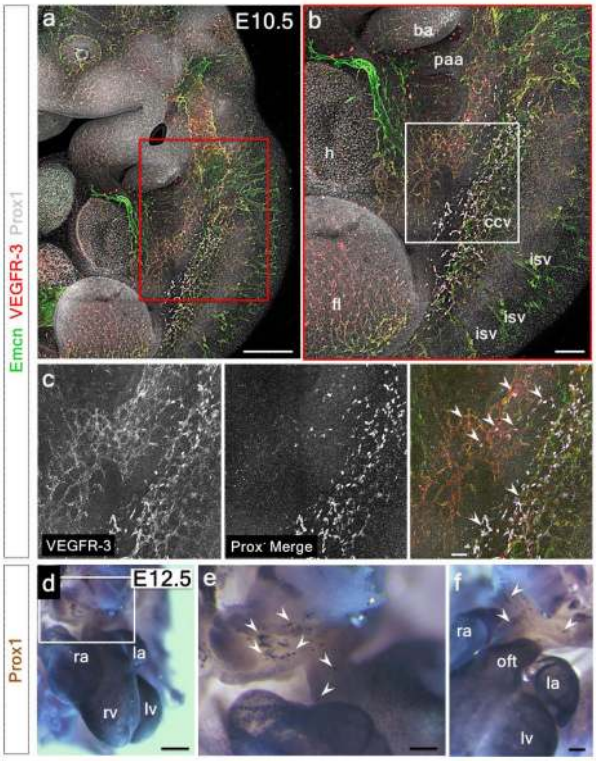

Extended Data Figure 3. The common cardinal vein contributes LECs that migrate towards the sinus venosus and outflow tract of the developing heart

Whole-mount confocal analysis of E10.5 embryos stained with Emcn or Prox1 and VEGFR-3 revealed Prox1/VEGFR-3+ LECs emerging along the common cardinal vein (**a**, red box enlarged in **b**; **b**, white box enlarged in **c**) migrating towards the sinus venosus (white arrowheads in **c**; n=3 embryos). Whole-mount DAB staining revealed Prox1+ LECs migrating towards the outflow tract, on the ventral surface of the developing heart at E12.5 (**d**, white inset box enlarged in **e**; alternative lateral view in **f**; white arrowheads indicate migrating LECs; n=4 embryos). **ba**, branchial arch; **ccv**, common cardinal vein; **fl**, forelimb; **h**, heart; **isv**, inter-somitic vessel; **la**, left atrium; **lv**, left ventricle; **oft**, outflow tract; **paa**,

pharyngeal artery arch; **ra**, right atrium; **rv**, right ventricle. Scale bars: **a** 1mm; **b** 500μm; **c** 200μm; **d** 600μm; **e** 400μm; **f** 300μm.

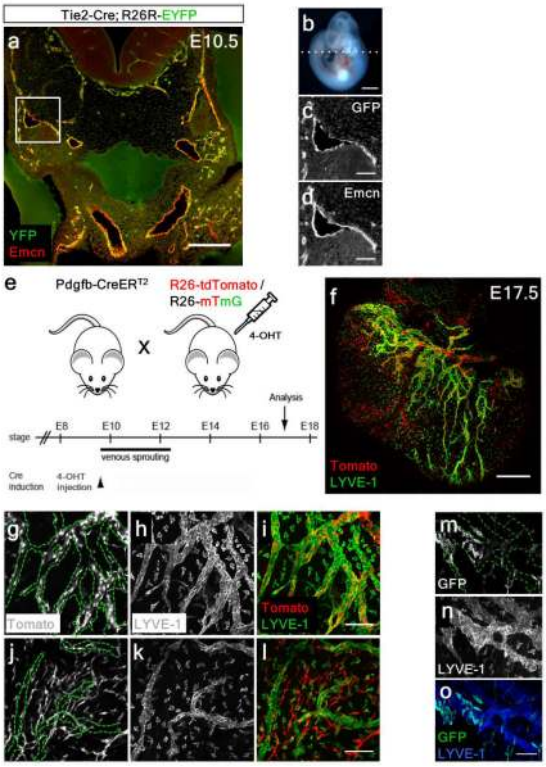

Extended Data Figure 4. TIE2-Cre efficiently labels the developing cardinal vein and partial contribution of PDGF-B+ derived LECs indicates a non-venous contribution to the developing cardiac lymphatics

TIE2-Cre;R26R-EYFP lineage tracing revealed recombination and labeling of the cardinal vein and jugular lymph sacs (**a)** at E10.5 (**b**; n=3 embryos analyzed). White inset box in (**a**) is shown at higher magnification and demarcated by α-GFP (**c**) and endomucin (Emcn; **d**) co-staining. Schematic (**e**) to show how embryos were generated by breeding PDGFB-CreER^{T2} mice with either R26R-tdTomato (**f**-**l**) or R26R-mTmG (**m**-**o**) reporter mice and injected with 4-Hydroxytamoxifen (4-OHT) at E9.5, prior to venous sprouting. Whole-mount confocal analysis of E17.5 hearts (n=4) stained with LYVE-1 revealed incomplete tdTomato recombination in cardiac lymphatic vessels (**f**). Both PDGF-B+ (**g**-**i**) and PDGF-B-negative (**j**-**l**; **m**-**o**) lymphatic vessels were observed, highlighted by the dotted green outlines (**g**, **j**, **m**), indicating a combined PDGF-B+ endothelial origin and PDGF-B-negative non-venous source for the cardiac LECs. Scale bars: **a** 200μm**; b** 1.5mm**; c**-**d** 50μm**; f** 400μm; **e, l, o** 100μm.

Europe PMC Funders Author Manuscripts

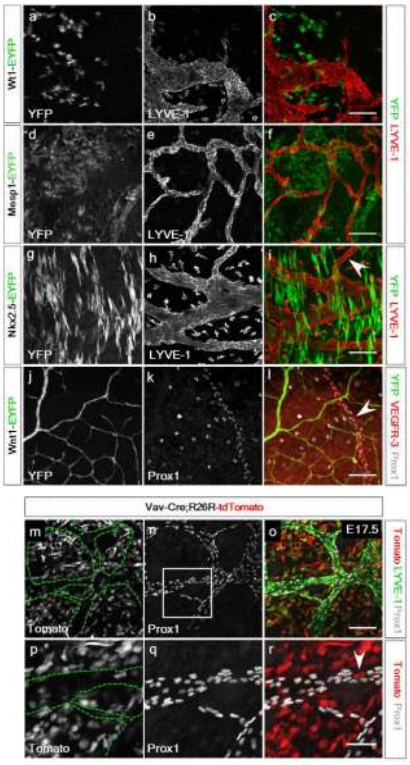

Extended Data Figure 5. Neither the pro-epicardial organ, cardiac mesoderm nor cardiac neural crest contribute LECs to the developing heart and dermal lymphatics are not derived from the Vav1+ lineage

Lineage tracing using WT1-CreERT2;R26R-EYFP (4-hydroxytamoxifen injected at E9.5; **a**-**c**), Mesp1-Cre;R26R-EYFP (**d**-**f**), Nkx2.5-Cre;R26R-EYFP (**g**-**i**) and Wnt1-Cre;R26R-EYFP (**j**-**l**; n=3 hearts analyzed per lineage trace) showed no YFP recombination in cardiac lymphatic vessels as marked by Prox1 or LYVE-1, suggesting that neither the pro-epicardial organ/epicardium, cardiac mesoderm (early or late) or cardiac neural crest, respectively, contribute LECs to the developing cardiac lymphatics.

Embryos generated by breeding Vav1-Cre with R26R-tdTomato reporter mice were subject to whole-mount confocal analysis of E17.5 of dorsal skin preparations (n=4 Vav1-tdTomato + embryos analyzed) for tdTomato epifluorescence (**m**) and Prox1 immunostaining (**n**) revealed a lack of Vav1-Cre recombination in dermal lymphatic vessels (highlighted by the green dotted lines, **m**) and a lack of overlap of Tomato with Prox1 and LYVE-1 expression (**o;** all Prox1+ nuclei assessed across 5 fields of view per embryonic skin; n=4 skins in total). Higher magnification of inset white box (**n**) revealed that Tomato+ cells (**p**) did not overlap with Prox1+ nuclei in the lymphatic vessels (**q**) (white arrowhead highlights Tomato +/Prox1-negative cell in **r**). Scale bars: **a**-**l**, 100μm; **m**-**o** 100μm; **p**-**r** 50μm.

Europe PMC Funders Author Manuscripts

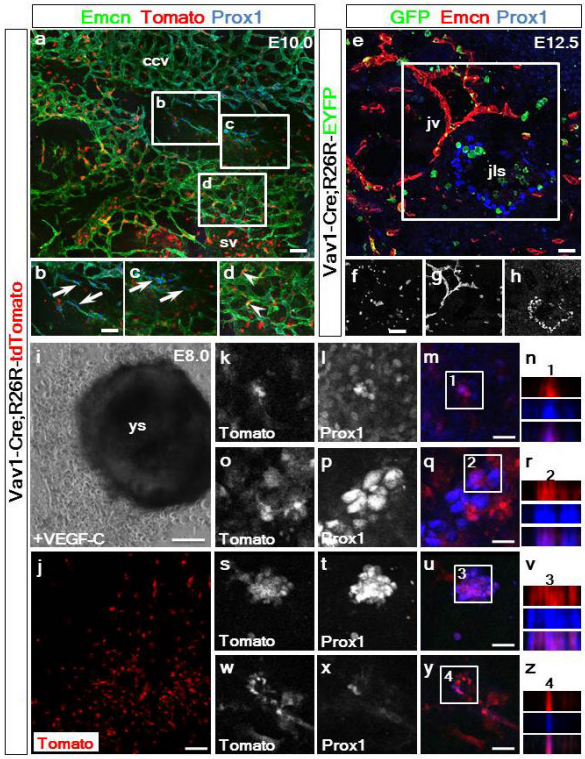

Extended Data Figure 6. The Vav1+ lineage does not contribute to LECs emerging from the common cardinal or jugular veins but contributes to VEGF-C induced LECs emerging from yolk sac explants

Vav1-Cre;R26R-tdTomato lineage tracing revealed no recombination nor labeling of the nascent LECs budding from common cardinal vein endothelium in E10.0 embryos (**a**) as confirmed by co-staining for Emcn, Prox1 and tdTomato fluorescence (**a**). White inset box in (**a**) highlighted by labeling for Emcn, Tomato and Prox1 (**b**-**d**). Vav1-Cre;R26R-EYFP lineage tracing revealed no recombination nor labeling of LECs forming the jugular lymph sacs in E12.5 embryos (**e)** as confirmed by co-staining for GFP, Emcn and Prox1 (**e**). White inset box in (**e**) highlighted by individual α-GFP (**f**), Emcn (**g**) and Prox1 (**h**) staining (n=3 embryos analyzed per time-point) **ccv**, common cardinal vein; **jls**, jugular lymph sac; **jv**, jugular vein; **sv**, sinus venosus. Representative staining for Prox1 and native Tomato fluorescence of *ex-vivo* cultures of explanted Vav1-Cre;R26R-tdTomato concepti at E8.0, including the intact yolk sac (**i**) and outgrowth of Tomato+ cells (**j**). Explants were cultured with 100ng/mL of recombinant VEGF-C-Cys(156)Ser[28] (R&D Systems), a potent selective lymphangiogenic cue that only signals via VEGFR-3 (**i**). High resolution images of the specification of Tomato+/Prox1+ LECs (indicated by white inset boxes) in the yolk sac explants (**k**-**n**) and in the surrounding cellular outgrowth (**o**-**z**) was observed (Tomato+ in red; Prox1+ in blue; single and merged channels shown). Co-staining was confirmed by z-stack reconstructions for each four high resolution panel set (**n**, **r**, **v**, **z**); n=6 explants analyzed. Scale bars: **a**, **e** 50μm; **b**-**d** and **f**-**h** 12.5μm; **i** 100μm; **j** 50μm; **m**, **q**, **u**, **y** 15μm

Europe PMC Funders Author Manuscripts

Europe PMC Funders Author Manuscripts

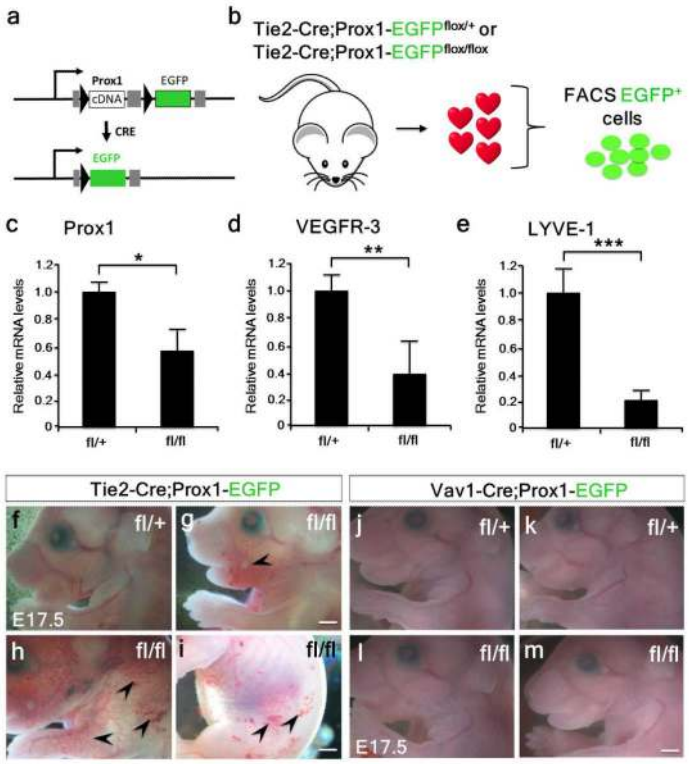

Extended Data Figure 7. *Prox1* knockdown results in significantly decreased *Vegfr3* and *Lyve1* and TIE2-CreProx1$^{fl/fl}$ mutant embryos exhibit superficial vascular defects whereas Vav1-Cre;Prox1$^{fl/fl}$ mutants have a normal systemic vasculature

Prox1 targeting via floxed excision of exon 1 and 2, results in EGFP expression thus labelling targeted cells (**a**). E17.5 hearts from either TIE2-Cre; Prox1$^{fl/+}$ control embryos or TIE2-Cre; Prox1$^{fl/fl}$ mutants were grouped and digested to create a single-cell suspension for FACS (**b**). A total of 100,000 GFP+ cells were collected for each sample group. Relative gene expression was determined by qRT-PCR and revealed significantly decreased *Prox1* (**c**; 0.59 fold), *Vegfr3* (**d**; 0.39 fold) and *Lyve1* expression (**e;** 0.22 fold); n=5 hearts per sample group, analyzed in triplicate; *p ≤0.05; **p ≤0.01; ***p ≤0.001. All graphs are mean ± s.e.m. All statistics Students't-test. Dissection of TIE2-Cre;Prox1$^{fl/+}$ heterozygous (**f**; n=6) and TIE2-Cre;Prox1$^{fl/fl}$ mutant (**g**, **h**, **i**; n=9) littermate embryos at E17.5, revealed gross vascular anomalies in the fl/fl mutants (three examples shown in **g-i**), with evidence of ectopic surface blood vessels (**g**, ectopic vessels highlighted by black arrowheads), a disrupted vascular network (**h**) and either hemorrhaging (**i**; bleeding foci highlighted by black arrowheads) or blood-filled lymphatics, compared to littermate controls fl/+ (**f**). Vav1-Cre;Prox1$^{fl/+}$ heterozygous (**j, k**; n=5) and Vav1-Cre;Prox1$^{fl/fl}$ mutants (**l, m**; n=8) revealed no obvious systemic vessel defects. Scale bars: **g**, **i, m** 100μm.

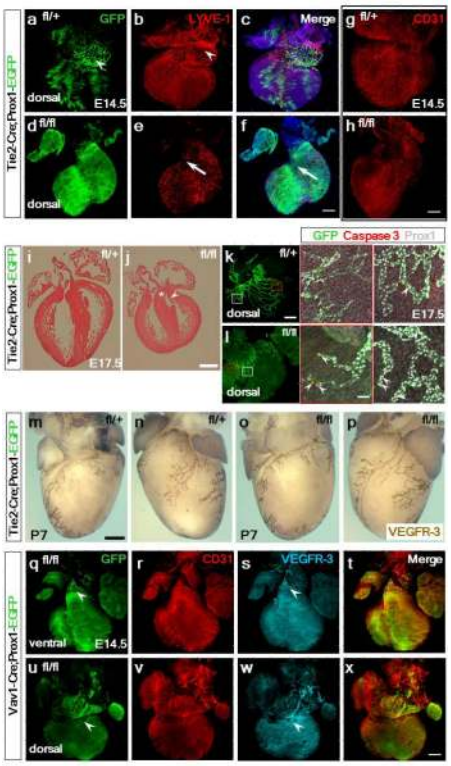

Extended Data Figure 8. The emergence of cardiac lymphatics at E14.5 is disrupted in TIE2-Cre;Prox1$^{fl/fl}$ mutant hearts, which are dysmorphic and exhibit elevated apoptosis of LECs, however, mutant embryos recover with normal cardiac lymphatics at post-natal stages

GFP+-targeted and LYVE-1+ LECs emerged from the base of the heart in the atrioventricular region at E14.5, in control TIE2-Cre;Prox1$^{fl/+}$ hearts (**a**-**c**; LECs highlighted by white arrowhead in **b**; n=3 hearts analyzed). In mutant TIE2-Cre;Prox1$^{fl/fl}$ hearts (n=7) the GFP+ network was absent (**d**) and LYVE-1 only detected tissue resident macrophages with an absence of lymphatics at the inflow base of the heart (arrows in **e**, **f**). Coronary vessels, as determined by whole mount CD31 staining, were comparable between control TIE2-Cre;Prox1$^{fl/+}$ (**g**) and Tie2-Cre;Prox1$^{fl/fl}$ hearts (**h**). Hematoxylin and eosin staining of paraffin-embedded of E17.5 hearts (**i**, **j**) revealed that TIE2-Cre;Prox1$^{fl/fl}$ mutants (**j**; n=3 analyzed) were grossly smaller compared to control hearts (**i**), with lack of extension of the ventricles towards the apex, smaller chambers and thickening of the ventricular free wall (**j**). Normal membranous septation of the mutant ventricle (white asterix) and valve leaflet formation (white arrowhead; **j**) indicate normal endocardial cushion development. Whole-mount confocal imaging of hearts stained with GFP, cleaved Caspase-3 and Prox1 revealed an increase in apoptotic cells within the termini of mutant coronary lymphatic vessels (magnified panels; white arrowheads), compared to control hearts (**k**, **l**; white arrowheads), supporting the requirement for Prox1 in LEC identity and maintenance. n=3 hearts analyzed for histology and immunostaining. Whole mount VEGFR-3 immunostaining of hearts isolated at post-natal day 7 (P7) revealed that TIE2-Cre;Prox1$^{fl/+}$ heterozygotes (**m**, **n**) and TIE2-Cre;Prox1$^{fl/fl}$ mutants (**o**, **p**) have an equivalent normal cardiac lymphatic vasculature (n=3 hearts analyzed per genotype). As such the lymphatic hypoplasia and disruption of the

Europe PMC Funders Author Manuscripts

vessel network, evident in mutant hearts at E17.5 (Extended Data Fig. 10), is rescued during the later stages of development and neonatal period.

In Vav1-Cre;Prox1$^{fl/fl}$ hearts (n=4) there was evidence of an initial formation of the cardiac lymphatics on both ventral (**q**, **s**) and dorsal (**u**, **w**) surfaces and the coronary vessels were unaffected (**r**, **t**, **v**, **x**). Scale bars: **f**, **h**, **x**, 400μm; **j** 1mm; **k** 400μm; **l** 50μm; **m**, 500μm.

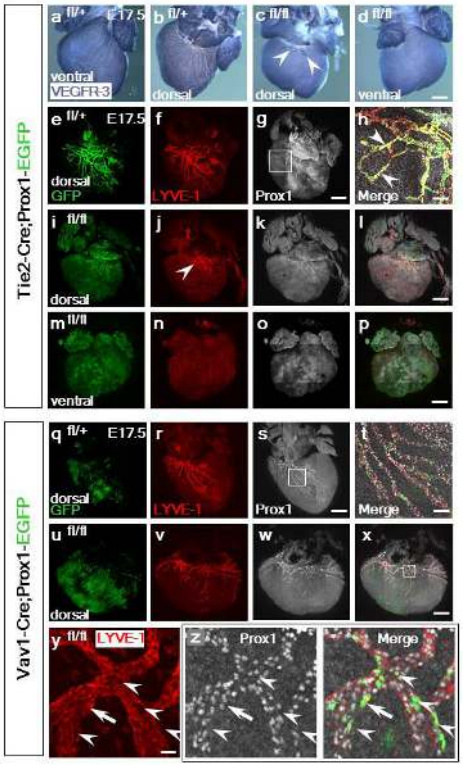

Extended Data Figure 9. Prox1 is essential for TIE2+ and Vav1+ derived cardiac lymphatics

In control TIE2-Cre;Prox1$^{fl/+}$ mice at E17.5 (n=6) there was an extensive lymphatic network on both the dorsal and ventral surfaces, as indicated by whole-mount VEGFR-3 immunostaining (**a**, **b**), whereas the lymphatic vessels were virtually absent in mutant TIE2-Cre;Prox1$^{fl/fl}$ hearts (**c**, **d**; n=9); a few vessels evident on the dorsal surface was consistent with LECs arising from a non-TIE2-targeted source (**c**, white arrowheads). TIE2-Cre;Prox1$^{fl/fl}$ mutant hearts were dysmorphic relative to controls (compare **c**, **d** with **a**, **b**). GFP+ staining indicated targeting of *Prox1* in TIE2-Cre;Prox1$^{fl/+}$ mice (**e**) and an expansive LYVE-1+ lymphatic network (**f**). Prox1 immunostaining confirmed expression in LECs in heterozygote controls (**g**; inset box shown at higher magnification in **h**). Co-expression of GFP/LYVE-1 and Prox1 was evident in LECs in addition to LYVE-1/Prox1 double positive cells not targeted by TIE2-Cre (**h**; white arrowheads). In contrast, TIE2-Cre;Prox1$^{fl/fl}$ mutant hearts revealed an absence of the GFP+ lymphatic network with only a minor contribution of LYVE-1 LECs evident at the base of the heart on the dorsal surface (**i**, **j**; white arrowhead in **j** highlights retained LYVE-1+ LECs), which were Prox1+ (**k**, **l**). On the ventral surface there was complete absence of GFP and LYVE-1+ lymphatic vessels (**m**); LYVE-1 staining was retained in tissue resident macrophages (**n**). Loss of LECs correlated with a loss of Prox1 (**o**, **p**). In control Vav1-Cre;Prox1$^{fl/+}$ mice at E17.5 (n=5) there was

evidence of appropriate targeting of GFP+ LECs (**q**) and an extensive lymphatic network on the dorsal surface as indicated by LYVE-1 (**r**). Prox1 expression was retained (**s**) which at higher resolution revealed co-expression of GFP+/LYVE-1+/Prox1+ in a subpopulation of LECs, consistent with the lineage trace data (Fig. 3a-d; white inset box in **s** shown at higher magnification in **t**). In Vav1-Cre;Prox1$^{fl/fl}$ mutant hearts (n=8) there was equivalent GFP+ targeting (**u**) and a LYVE-1+ network (**v**) with retained Prox1 expression (**w**, **x**). Specific loss of LYVE-1 staining (**y**) correlated with loss of Prox1 and GFP-targeting (**z**, left and right hand panels, respectively, highlighted by white arrowheads). Mosaic levels of Prox1 knock-down accounted for examples of isolated LECs that, despite GFP-targeting, remained LYVE-1+ (white arrows; **y**, **z**). Scale bars: **d**, **g, l, p, s, x,** 400μm; **h**, **t**, 40μm; **y**, 5μm.

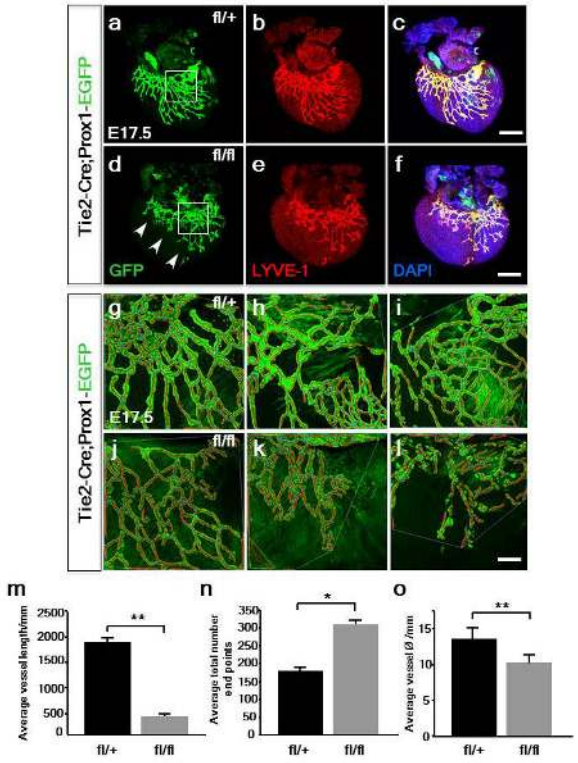

Extended Data Figure 10. Prox1 knockdown in TIE2-Cre;Prox1$^{fl/fl}$ mutants results in a hypoplastic and disrupted lymphatic plexus

Relative to Tie2-Cre;Prox1$^{fl/+}$ control hearts at E17.5 (**a**-**c**), GFP+ lymphatic vessels were thinner and the network truncated along the short axis, having failed to appropriately extend and remodel in TIE2-Cre;Prox1$^{fl/fl}$ hearts with partial knock-down of *Prox1* (**d**-**f**; see Extended Data Fig. 7**c**; n= 4 hearts per genotype; representative regions indicated by white inset boxes in **a**, **d**). Higher magnification of the lymphatic plexus in TIE2-Cre;Prox1$^{fl/+}$ control (**g**-**i**) and TIE2-Cre;Prox1$^{fl/fl}$ mutants (**j**-**l**) were captured for AngioTool analyses. AngioTool tracing in red of GFP+ vessels and blue for branch points (**g**-**l**), enabled quantitative assessment of vessel parameters. The mutant lymphatic vessels were significantly shorter in overall length (**m**), more truncated and disorganized with an increased total number of end points (**n**). Mutant vessels were also significantly reduced in diameter, being thinner on average, compared to controls (**o**). Scale bars: **c**, **f,** 400μm; **l,**

30mm; All graphs show mean ± s.e.m. Student's t-test; *p ≤0.05; **p ≤0.001 (n=4 hearts analyzed per genotype).

Supplementary Material

Refer to Web version on PubMed Central for supplementary material.

Acknowledgements

This work was funded by the Wellcome Trust (LK), EU FP7 Marie Curie ITN (CardioNet; MM) and the British Heart Foundation (SN, JMV, MR, KD, SB, CAC, PRR). We thank J. Pollard for providing the *Csf1r-CreER* mouse line, K. Alitalo for providing the *Vegfr3*$^{LacZ/+}$ mouse line, T. Makinen for providing *Pdgfrβ-Cre* embryos and the transgenic services at the University of Oxford for rederiving the *Prox1*$^{flox/+}$ mouse line from RIKEN (accession number CDB0482K). We are grateful to B. Vernay and A. Eddaoudi for assistance with confocal microscopy and flow cytometry, respectively.

References

1. Sabin F. On the origin of the lymphatic system from the veins and the development of the lymph hearts and thoracic duct in the pig. American Journal of Anatomy. 1902; 1:367.
2. Huntington GSM, C FW. The anatomy and development of the jugular lymph sac in the domestic cat. American Journal of Anatomy. 1910; 10:177.
3. Srinivasan RS, et al. Lineage tracing demonstrates the venous origin of the mammalian lymphatic vasculature. Genes Dev. 2007; 21:2422–32. [PubMed: 17908929]
4. Yaniv K, et al. Live imaging of lymphatic development in the zebrafish. Nat Med. 2006; 12:711–6. [PubMed: 16732279]
5. Yang Y, et al. Lymphatic endothelial progenitors bud from the cardinal vein and intersomitic vessels in mammalian embryos. Blood. 2012; 120:2340–8. [PubMed: 22859612]
6. Okuda KS, et al. lyve1 expression reveals novel lymphatic vessels and new mechanisms for lymphatic vessel development in zebrafish. Development. 2012; 139:2381–91. [PubMed: 22627281]
7. Hagerling R, et al. A novel multistep mechanism for initial lymphangiogenesis in mouse embryos based on ultramicroscopy. EMBO J. 2013; 32:629–44. [PubMed: 23299940]
8. Flaht A, et al. Cellular phenotypes and spatio-temporal patterns of lymphatic vessel development in embryonic mouse hearts. Dev Dyn. 2012; 241:1473–86. [PubMed: 22753134]
9. Joukov V, et al. A novel vascular endothelial growth factor, VEGF-C, is a ligand for the Flt4 (VEGFR-3) and KDR (VEGFR-2) receptor tyrosine kinases. EMBO J. 1996; 15:1751. [PubMed: 8612600]
10. Wigle JT, Oliver G. Prox1 function is required for the development of the murine lymphatic system. Cell. 1999; 98:769–778. [PubMed: 10499794]
11. Buttler K, Ezaki T, Wilting J. Proliferating mesodermal cells in murine embryos exhibiting macrophage and lymphendothelial characteristics. BMC Dev Biol. 2008; 8:43. [PubMed: 18430230]
12. Koni PA, et al. Conditional vascular cell adhesion molecule 1 deletion in mice: impaired lymphocyte migration to bone marrow. J Exp Med. 2001; 193:741–54. [PubMed: 11257140]
13. Srinivas S, et al. Cre reporter strains produced by targeted insertion of EYFP and ECFP into the ROSA26 locus. BMC.Dev.Biol. 2001; 1:4. [PubMed: 11299042]
14. Madisen L, et al. A robust and high-throughput Cre reporting and characterization system for the whole mouse brain. Nat Neurosci. 2010; 13:133–40. [PubMed: 20023653]
15. Muzumdar MD, Tasic B, Miyamichi K, Li L, Luo L. A global double-fluorescent Cre reporter mouse. Genesis. 2007; 45:593–605. [PubMed: 17868096]
16. Brade T, Pane LS, Moretti A, Chien KR, Laugwitz KL. Embryonic Heart Progenitors and Cardiogenesis. Cold Spring Harb Perspect Med. 2013; 3

17. Zhou B, et al. Epicardial progenitors contribute to the cardiomyocyte lineage in the developing heart. Nature. 2008; 454:109–113. [PubMed: 18568026]
18. Saga Y, et al. MesP1 is expressed in the heart precursor cells and required for the formation of a single heart tube. Development. 1999; 126:3437–3447. [PubMed: 10393122]
19. Moses KA, DeMayo F, Braun RM, Reecy JL, Schwartz RJ. Embryonic expression of an Nkx2-5/Cre gene using ROSA26 reporter mice. Genesis. 2001; 31:176–180. [PubMed: 11783008]
20. Jiang X, Rowitch DH, Soriano P, McMahon AP, Sucov HM. Fate of the mammalian cardiac neural crest. Development. 2000; 127:1607–1616. [PubMed: 10725237]
21. Tang Y, Harrington A, Yang X, Friesel RE, Liaw L. The contribution of the Tie2+ lineage to primitive and definitive hematopoietic cells. Genesis. 2010; 48:563–7. [PubMed: 20645309]
22. Georgiades P, et al. VavCre transgenic mice: a tool for mutagenesis in hematopoietic and endothelial lineages. Genesis. 2002; 34:251–6. [PubMed: 12434335]
23. Chen MJ, Yokomizo T, Zeigler BM, Dzierzak E, Speck NA. Runx1 is required for the endothelial to haematopoietic cell transition but not thereafter. Nature. 2009; 457:887–91. [PubMed: 19129762]
24. Ruiz-Herguido C, et al. Hematopoietic stem cell development requires transient Wnt/beta-catenin activity. J Exp Med. 2012; 209:1457–68. [PubMed: 22802352]
25. Rolny C, et al. Platelet-derived growth factor receptor-beta promotes early endothelial cell differentiation. Blood. 2006; 108:1877–86. [PubMed: 16690964]
26. Perdiguero EG, et al. Tissue-resident macrophages originate from yolk-sac-derived erythro-myeloid progenitors. Nature. 2014
27. Hamada K, et al. VEGF-C signaling pathways through VEGFR-2 and VEGFR-3 in vasculoangiogenesis and hematopoiesis. Blood. 2000; 96:3793–800. [PubMed: 11090062]
28. Breslin JW, et al. Vascular endothelial growth factor-C stimulates the lymphatic pump by a VEGF receptor-3-dependent mechanism. Am J Physiol Heart Circ Physiol. 2007; 293:H709–18. [PubMed: 17400713]
29. Iwano T, Masuda A, Kiyonari H, Enomoto H, Matsuzaki F. Prox1 postmitotically defines dentate gyrus cells by specifying granule cell identity over CA3 pyramidal cell fate in the hippocampus. Development. 2012; 139:3051–3062. [PubMed: 22791897]
30. Kataru RP, et al. Critical role of CD11b+ macrophages and VEGF in inflammatory lymphangiogenesis, antigen clearance, and inflammation resolution. Blood. 2009; 113:5650–9. [PubMed: 19346498]
31. Huggenberger R, et al. An important role of lymphatic vessel activation in limiting acute inflammation. Blood. 2011; 117:4667–4678. [PubMed: 21364190]
32. Nahrendorf M, et al. The healing myocardium sequentially mobilizes two monocyte subsets with divergent and complementary functions. J.Exp.Med. 2007; 204:3037–3047. [PubMed: 18025128]
33. Smart N, et al. De novo cardiomyocytes from within the activated adult heart after injury. Nature. 2011; 474:640–644. [PubMed: 21654746]
34. Dumont DJ, et al. Cardiovascular failure in mouse embryos deficient in VEGF receptor-3. Science. 1998; 282:946–9. [PubMed: 9794766]
35. Tammela T, et al. Therapeutic differentiation and maturation of lymphatic vessels after lymph node dissection and transplantation. Nat Med. 2007; 13:1458–66. [PubMed: 18059280]
36. Wigle JT, et al. An essential role for Prox1 in the induction of the lymphatic endothelial cell phenotype. EMBO J. 2002; 21:1505–1513. [PubMed: 11927535]
37. Petrova TV, et al. Lymphatic endothelial reprogramming of vascular endothelial cells by the Prox-1 homeobox transcription factor. EMBO J. 2002; 21:4593–9. [PubMed: 12198161]
38. Johnson NC, et al. Lymphatic endothelial cell identity is reversible and its maintenance requires Prox1 activity. Genes & Development. 2008; 22:3282–3291. [PubMed: 19056883]
39. Kim H, et al. Embryonic vascular endothelial cells are malleable to reprogramming via Prox1 to a lymphatic gene signature. BMC Dev Biol. 2010; 10:72. [PubMed: 20584329]
40. Kazenwadel J, Michael MZ, Harvey NL. Prox1 expression is negatively regulated by miR-181 in endothelial cells. Blood. 2010; 116:2395–2401. [PubMed: 20558617]

41. Srinivasan RS, Oliver G. Prox1 dosage controls the number of lymphatic endothelial cell progenitors and the formation of the lymphovenous valves. Genes Dev. 2011; 25:2187–97. [PubMed: 22012621]
42. Karkkainen MJ, Jussila L, Ferrell RE, Finegold DN, Alitalo K. Molecular regulation of lymphangiogenesis and targets for tissue oedema. Trends Mol Med. 2001; 7:18–22. [PubMed: 11427983]
43. Szuba A, et al. Therapeutic lymphangiogenesis with human recombinant VEGF-C. FASEB J. 2002; 16:1985–7. [PubMed: 12397087]
44. Saga Y, et al. MesP1 is expressed in the heart precursor cells and required for the formation of a single heart tube. Development. 1999; 126:3437–47. [PubMed: 10393122]
45. Claxton S, et al. Efficient, inducible Cre-recombinase activation in vascular endothelium. Genesis. 2008; 46:74–80. [PubMed: 18257043]
46. Foo SS, et al. Ephrin-B2 controls cell motility and adhesion during blood-vessel-wall assembly. Cell. 2006; 124:161–73. [PubMed: 16413489]
47. de Boer J, et al. Transgenic mice with hematopoietic and lymphoid specific expression of Cre. Eur J Immunol. 2003; 33:314–25. [PubMed: 12548562]
48. Zudaire E, Gambardella L, Kurcz C, Vermeren S. A computational tool for quantitative analysis of vascular networks. PLoS One. 2011; 6:e27385. [PubMed: 22110636]
49. Schneider JE, et al. Fast, high-resolution in vivo cine magnetic resonance imaging in normal and failing mouse hearts on a vertical 11.7 T system. J Magn Reson Imaging. 2003; 18:691–701. [PubMed: 14635154]
50. Carr CA, et al. Bone marrow-derived stromal cells home to and remain in the infarcted rat heart but fail to improve function: an in vivo cine-MRI study. Am J Physiol Heart Circ Physiol. 2008; 295:H533–42. [PubMed: 18539761]

Europe PMC Funders Author Manuscripts

Europe PMC Funders Author Manuscripts

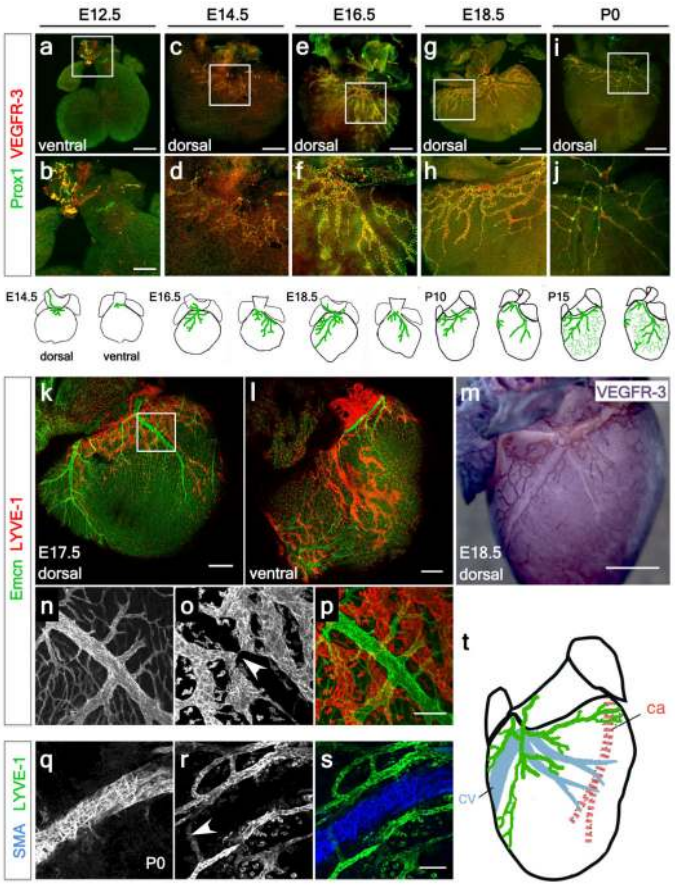

Figure 1. Spatiotemporal development of the murine cardiac lymphatic vasculature

Whole-mount confocal imaging of embryonic hearts stained with VEGFR-3 and Prox1 at E12.5 (**a**, white box, enlarged in **b**), E14.5 (**c**, white box, enlarged in **d**), E16.5 (**e**, enlarged box in **f**) and E18.5 (**g**, enlarged box in **h**). From birth, post-natal day (P) 0, lymphatic vessels branch and expand further onto the dorsal epicardial surface of the heart (**i**, enlarged box in **j**). Schematics represent the stages of lymphatic vessel development (n=5 hearts analyzed per time point). Whole-mount staining with endomucin (Emcn, veins) and LYVE-1 (lymphatics) (**k**-**l**) and DAB staining with VEGFR-3 (**m**), (**n**-**p**, white arrowhead in **o** highlights a coronary vein). Alpha-smooth muscle actin (SMA) stained hearts (veins) and LYVE-1 (lymphatics) (**q**-**s**; white arrowhead indicates location of blood vessels, **r**) at later stages (P0) with accompanying schematic representation of the dorsal side the heart at P10 (shown in Extended Data Fig. 1**g**, **h;** n= 5 hearts analyzed per time point). Scale bars: **a, c, e** 750μm; **b** 300μm, **g** 1mm; **i** 2mm; **k**-**m**, 200μm; **p** 10μm; **s** 5μm.

Europe PMC Funders Author Manuscripts

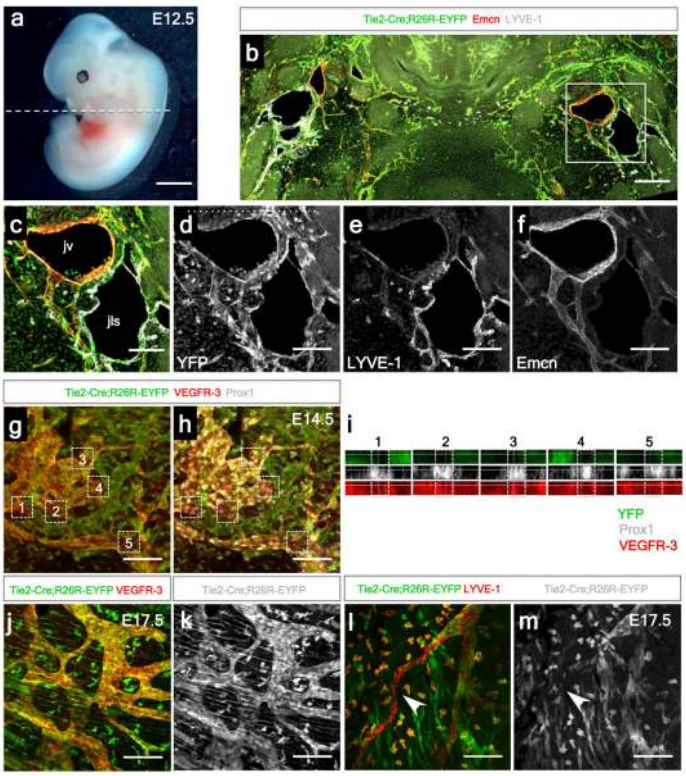

Figure 2. Incomplete contribution of TIE2+ venous-derived LECs indicates a novel non-venous contribution to the developing cardiac lymphatics

Tie2-Cre;R26R-EYFP embryos at E12.5 (**a**) stained with anti-GFP, LYVE-1 and Endomucin antibodies (Emcn; **b**-**f**). Jugular lymph sacs were YFP+ **(b, c).** Whole-mount staining with VEGFR-3, LYVE-1, or Prox1 revealed incomplete recombination in cardiac lymphatic vessels (**g**) with evident YFP-negative regions of vasculature containing Prox1^{+} nuclei (**h**); see confocal z-stack reconstructions numbered 1-5 (**i**, as indicated by white inset boxes; **g**, **h**). At E17.5, both TIE2-YFP+ vessels (**j**, **k**) and TIE2-YFP− vessels were observed (**l, m**; highlighted by white arrowheads); n=5 hearts analyzed per time point. Scale bars: **a**, 200μm; **b**-**m**, 100μm.

Europe PMC Funders Author Manuscripts

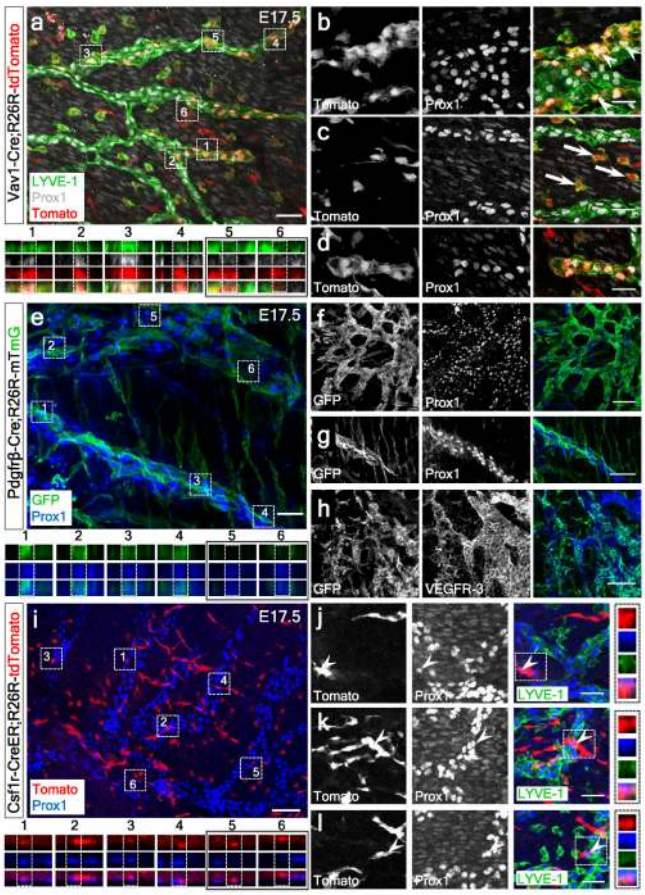

Figure 3. Vav1+, PDGFRβ+ and CSF1R+ lineages contribute LECs to the developing cardiac lymphatics

Vav1-Cre;R26R-tdTomato lineage tracing revealed regions of Tomato+ recombination throughout the heart at E17.5 (**a**; n=4 hearts analyzed). Tomato+, Prox1+ and LYVE-1^{+} cardiac lymphatic vessels were traced at E17.5 (**b**-**d**; white arrowheads in **b**) and co-labelled Tomato+/Prox1+/LYVE-1+ were confirmed by z-stack reconstructions (**a**, 1-4; 5, 6 lack Prox1 and are Tomato+/LYVE-1+ macrophages). Macrophages proximal to the Prox1+ LECs were evident at higher magnification (**c**; white arrows). PDGFRβ-Cre; R26R-mTmG E17.5 hearts including z-stack reconstruction (**e**; stacks 1-4 are GFP+/Prox1+; 5, 6 are single Prox1+; n=3 hearts analyzed) revealed a heterogeneous contribution of recombined GFP+ cells that were Prox1+ (**f**, **g**) or VEGFR3+ (**h**). Analyses of E17.5 hearts from CSF1R-CreER;R26R-tdTomato embryos injected with 4-hydroxytamoxifen at E7.5 (**i**; n=5 hearts analyzed) revealed contribution of recombined tdTomato+ cells that were Prox1+ (**i-l**; z-stack projections 1-4 in **i** and white arrowheads in **j**-**l** with accompanying z-stacks). Scale bars: **a, e, i** 60μm; **b**-**d**, 30μm; **f**, **h**, **j**, **k**, **l** 100μm; **g**, 200μm.

Europe PMC Funders Author Manuscripts

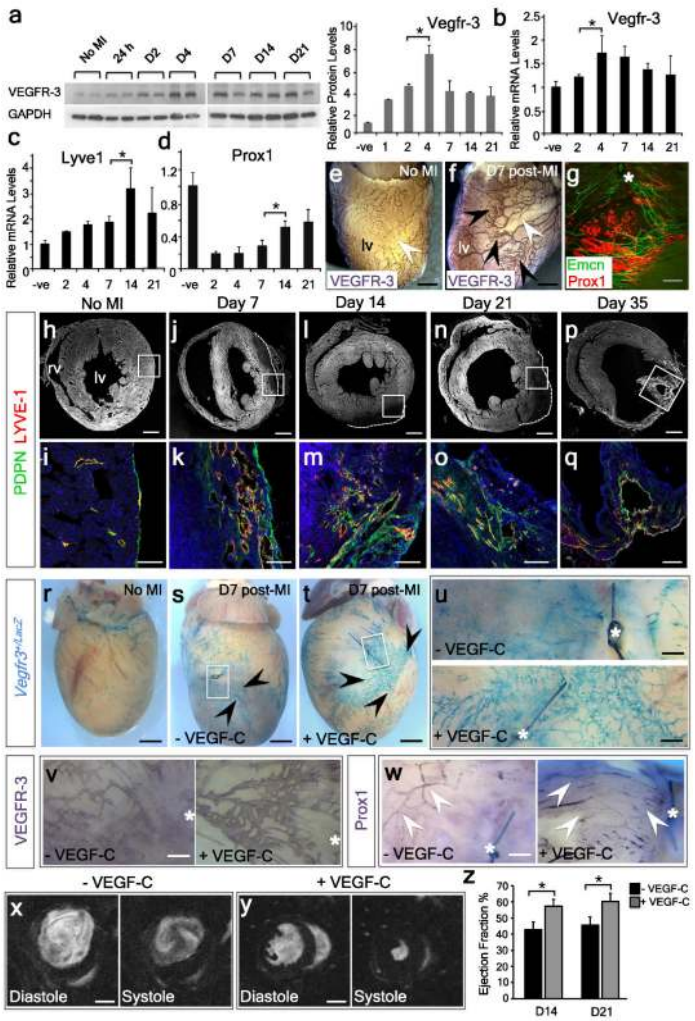

Figure 4. Myocardial infarction induces a significant cardiac lymphangiogenic response that can be enhanced by VEGF-C-stimulation to promote functional improvement

VEGFR-3 protein levels increased from 24h to 21 days post-MI, peaking at day 4 (**a**; n=3 animals analyzed per time point; single representative western blot with densitometry shown in **a**). Real-time analysis of *Vegfr3* (**b**), *Lyve1* (**c**) and *Prox1* (**d**), all revealed a significant increase in expression levels across the equivalent time-points post-MI (n=3 animals per time-point). VEGFR-3 whole mount staining, revealed increased lymphangiogenesis in the left ventricle (lv), proximal to the infarct after 7 days post-MI (**e, f**; n=3 mice per group). Sprouting of Prox1+ lymphatics was observed aligning with Emcn+ veins after 7 days post-MI (**g**, white asterisk; ligating suture). Short axis sections at day 7 post-MI revealed LYVE-1+/podoplanin (PDPN)+ lymphangiogenesis in the scar region (white boxes in **h**, **j, l, n, p**), which was significantly increased relative to the intact heart (**h**, **i**) and which expanded through days 14 (**m**), 21 (**o**) and 35 with large lymphatic ‘shunts’ evident in the lv (**q**; n=5 hearts analyzed). Whole-mount X-gal staining of *Vegfr3*$^{+/LacZ}$ hearts post administration of VEGF-C reported the lymphangiogenic response post-MI (**r**-**u**; n=3 per treatment group). Mice treated with recombinant human VEGF-C (Cys156Ser; **t**) exhibited extensive lymphangiogenesis in the injury area (black arrowheads and white inset box enlarged in **u**)

compared with vehicle-treated (**s**; black arrowheads and white inset box enlarged in **u**) or sham-operated mice (**r**). Whole-mount DAB staining of MI hearts +/− VEGF-C administration, with VEGFR-3 (**v**) or Prox-1 (**w**) confirmed the observations in **r**-**u (**the white asterisk indicates the ligating suture). Longitudinal MRI analyses of infarcted hearts 21 days after surgery following treatment with either vehicle (**x**) or VEGF-C (**y**). Ejection fraction measurements (%) revealed a significant improvement in VEGF-C-treated hearts, compared to vehicle, at 14 and 21 days post-MI (**z**). n=8 wild-type mice per treatment group. All graphs show mean ± s.e.m. All statistics Student's t-test; * $p \leq 0.05$; Scale bars: **e**, **f** 1mm; **g** 400μm; **h, j, l, n, p**, 200μm; **i, k, m, o, q** 400μm; **r-t** 1mm; **u-w** 500μm; **x**, **y** 2mm.

Europe PMC Funders Author Manuscripts